JOURNAL OF MATERIALS SCIENCE **35** (2000) 6065–6074

# Microstructural aspects of the fracture process in human cortical bone

O. AKKUS, K. J. JEPSEN, C. M. RIMNAC*
*Musculoskeletal Biomechanics and Orthopaedic Engineering Laboratories, Department of Mechanical and Aerospace Engineering, Case Western Reserve University,*
*10900 Euclid Avenue, Cleveland, OH 44106-7222, USA*
*E-mail: cmr10@po.cwru.edu*

Fracture toughness tests were conducted in the transverse and longitudinal directions to the osteonal orientation of human femoral cortical bone tissue to investigate the resulting damage patterns and their interaction with the microstructure. The time history of damage accumulation was monitored with acoustic emission (AE) during testing and was spatially observed histologically following testing. The fracture toughness of the transverse specimens was almost two times greater than the fracture toughness of the longitudinal specimens (3.47 $\mathrm{MNm}^{-3/2}$ vs. 1.71 $\mathrm{MNm}^{-3/2}$, respectively). The energy content of the AE waveforms of transverse specimens were greater than those of the longitudinal specimens implying higher fracture resistance in the transverse crack growth direction. The results showed that the propagation of the main crack involved weakening of the tissue by ultrastructural (diffuse) damage at the fracture plane and formation of linear microcracks away from the fracture plane for the transverse specimens. For the longitudinal specimens, the growth of the main crack occurred in the form of separations at lamellar interfaces. The lamellar separations generally arrested at the cement lines. Linear microcracks occurred primarily in the interstitial tissue for both crack growth directions. *© 2000 Kluwer Academic Publishers*

## 1. Introduction

The fracture process in composite materials occurs as an accumulation of microscopic cracks followed by their coalescence into macrocracks [1, 2]. Like synthetic composite materials, damage in the form of microcracks has also been observed in cortical bone following *in-vivo* or *in-vitro* loading [3–6]. The location of these microcracks within the microstructure of cortical bone has been extensively investigated [7, 8] and the degradation of the material properties of cortical bone due to microcrack accumulation has been demonstrated [4, 5, 9–11]. However, the manner by which microcracks coalesce, grow and interact with the microstructure in relation to fracture of cortical bone tissue is not well understood. Gaining insight into microcrack coalescence and growth is integral to the understanding of the fracture of human cortical bone. Furthermore, the fracture of normal bone tissue needs to be understood to understand fractures due to aging, exercise, over-use and disease.

The objective of the current study was to investigate both qualitative and quantitative aspects of the coalescence and growth of microcracks, as well as their interaction with the microstructure to provide additional insight into the mechanisms of fracture of human cortical bone. For this purpose, fracture toughness tests were conducted in the transverse and longitudinal directions to osteonal orientation to investigate the effect of microstructure on the fracture resistance of cortical bone. During testing, the time history of the formation of damage and growth of the main crack was monitored with acoustic emission and spatial information about damage was evaluated by histology following testing.

## 2. Materials and methods

Cortical specimens were obtained from the diaphyses of the left and right femora of a 53 year old female donor (Musculoskeletal Transplant Foundation, Edison NJ) who had no known skeletal pathologies. Wafers, 3 mm in thickness, were cut in the longitudinal-tangential plane of the diaphysis using a low speed saw (Buehler, Lake Bluff IL). Compact tension specimens were then machined from the wafers. The specimen width, $W$, was 14 mm and the crack length to width ratio, $a/W$, was 0.25 (Fig. 1). The notch was machined either parallel (longitudinal, $n = 3$) or perpendicular (transverse, $n = 4$) to the osteonal orientation with a low speed saw. Grooves were machined on both faces, leaving 1.5 mm thickness between the grooves (Fig. 1). Each specimen was precracked using a razor blade attached to a microtome (American Optical Co., Buffalo NY) via custom

---

* Author to whom all correspondence should be addressed.

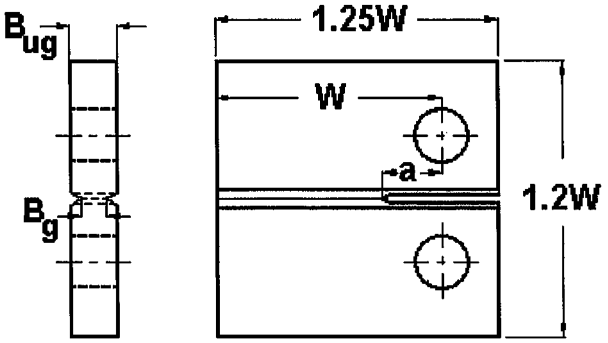

*Figure 1* Schema of the grooved compact tension specimen. $W = 14$ mm, $a/W = 0.25$. $B_{ug} \cong 3$ mm and $B_g \cong 1.5$ mm are the ungrooved and grooved thickness of the specimen, respectively.

made fixtures. The razor was aligned with the plane of the groove and the specimen was precracked in 5 $\mu$m increments along a distance of 500 $\mu$m. The specimens were kept wet in distilled water during all machining and preparation stages. The specimens were kept frozen in distilled water until testing.

## 2.1. Fracture toughness testing and acoustic emission

Prior to fracture toughness testing, two acoustic emission (AE) transducers (T1 and T2, Fig. 2) were coupled to the specimens with cyanoacrylate glue. The specimens were loaded in a servohydraulic testing machine (Instron, Canton MA) at a displacement rate of 0.09 mm/min using fixtures that conformed to ASTM Standard E399-90 [12]. The specimens were kept wet throughout testing using a continuous saline drip at ambient temperature. AE signals were amplified 40 dB (PA1 and PA2, Fig. 2). The amplified signal was sampled at a rate of 8 MHz using an AE data acquisition board (AEDSP 32/16, Physical Acoustics Corporation, Princeton NJ) and recorded on a personal computer in real time. The threshold of acquisition was set at 45 dB to eliminate false triggers due to extraneous noise. Loading was stopped when the load value dropped below 10 N for the longitudinal and 30 N for the transverse specimens. Histological observation following fracture toughness tests confirmed that all cracks propagated at least 8 mm ($a = 11.5$ mm, Fig. 1) in all specimens.

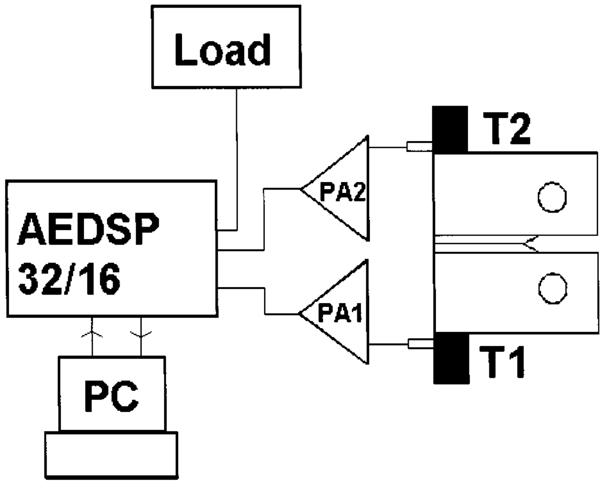

*Figure 2* Acoustic emission test set up.

The critical stress intensity factor ($K_c$) was calculated from the load-displacement curve, as reported previously by others [13, 14]. The critical stress intensity factor ($K_c$) was defined as:

$$K_c = \frac{P_c}{BW^{1/2}} f(a/W) \tag{1}$$

Where

$$\begin{aligned} f(a/W) = {} & (2 + a/W)^*(0.886 + 4.64a/W \\ & - 13.32a^2/W^2 + 14.72a^3/W^3 \\ & - 5.6a^4/W^4)/(1 - a/W)^{3/2} \end{aligned} \tag{2}$$

$$B = (B_g B_{ug})^{1/2} \tag{3}$$

Where $P_c$ is the critical load, $a$ is the initial crack length, $W$ is the specimen width, $B_{ug}$ is the ungrooved specimen thickness, and $B_g$ is the grooved thickness (Fig. 1). $P_c$ was obtained by taking the intersection of the load displacement curve with a secant line through the origin having a slope that was 5% less than the slope of the initial linear portion of the load displacement curve [12]. Average $K_c$ values for the transverse and longitudinal groups were compared by the Mann-Whitney test ($p < 0.05$).

## 2.2. Histological evaluation

Following mechanical testing, specimens were fixed in 70% ethanol overnight and bulk stained in 1% basic fuchsin [15]. Specimens were embedded in poly(methylmethacrylate) and sectioned to 250 $\mu$m thickness using a diamond coated saw. The sections were glued to acrylic plates and ground to 150 $\mu$m thickness. Final polishing was performed with 1 $\mu$m diamond suspension.

Three sections were obtained from the transverse specimens: one section was taken as close as possible to the fracture plane; and, two sections were taken 0.85 mm above and 0.85 mm below the fracture plane (Fig. 3). Five sections were taken from the longitudinal specimens perpendicular to the crack propagation

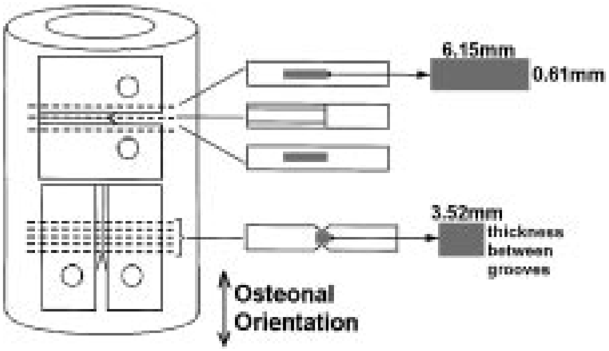

*Figure 3* Location of histological sections taken from the compact tension specimens. All sections were taken transversely to the osteonal orientation. A top view of the sections is shown on the right. The shaded regions show the areas that were histologically quantified.

direction every 0.85 mm, starting from the crack tip (Fig. 3). Thus, for both specimen orientations, the sections were taken perpendicular to the osteons.

Microcrack counting was performed manually using transmitted light microscopy at 200× magnification for the sections from the transverse specimens and at 100× magnification for the sections from the longitudinal specimens. Different magnifications were required to accommodate the differences in the crack lengths between the transverse and longitudinal specimens.

The microcracks that were counted were defined as linear (or curvilinear) structures showing increased dye penetration in comparison to the tissue surrounding them. Macroscopically visible cracks were not counted, nor were submicroscopic cracks below the resolution of the magnification at which the counting was being conducted. Thus, microcracks were defined as cracks that were visible at the microscope eyepiece at the given magnifications.

The number of microcracks for each section was counted in the regions highlighted in Fig. 3. For the transverse sections, the region was evaluated by counting microcracks in 15 contiguous fields. For the longitudinal specimens, the region was evaluated by counting microcracks in 8 contiguous fields. Microcrack counting was not performed on the fracture plane sections of the transverse specimens due to excessive damage; however the fracture plane sections were qualitatively evaluated.

Three types of microcracks were classified on the basis of their location in the microstructure: microcracks within the interstitial tissue (IT); microcracks within osteons (O); and microcracks along cement lines (CL). The number of microcracks for a section was divided by the area of observation to obtain the numerical density of microcracks (Cr.De., #/mm$^2$). Differences between the microcrack densities for the three different microstructural locations (IT, O, and CL) were determined by the Mann-Whitney test ($p < 0.1$).

### 2.3. Identification of failure modes by clustering of acoustic emission waveforms

Using MISTRAS software (Physical Acoustics Corporation, Princeton NJ), four waveform features were extracted: amplitude (AM), counts (CO), rise time (RT), and duration (DU) (Fig. 4). A triangle, referred to as an envelope detected waveform (EDW) [16] was constructed by using the four waveform features (Fig. 4). An EDW approximates the shape of the waveform in terms of waveform features. Six pattern parameters were then calculated for each EDW: total amplitude ($A_T$); total energy ($E_T$), 1st order amplitude and energy moments ($A^{(1)}$) and ($E^{(1)}$), respectively; and 2nd order amplitude and energy moments ($A^{(2)}$) and ($E^{(2)}$), respectively (Fig. 4). Pattern parameters were utilized to define the shape characteristics of a waveform, such as the symmetry ($A^{(1)}$ and $E^{(1)}$) and the peakedness ($A^{(2)}$ and $E^{(2)}$) [16].

Each EDW was treated as a single observation that was defined using selected variables taken from the waveform features and the pattern parameters: CO, $E_T$, $A^{(1)}$, $E^{(1)}$, $A^{(2)}$, $E^{(2)}$. The waveform features of amplitude, duration, and rise time are accounted for in the pattern parameters, and were thus, not included as variables. The total amplitude, $A_T$, was also not included as a variable because it is highly correlated with the total energy, $E_T$. The EDW's recorded during the fracture of the transverse and longitudinal specimens were pooled for each orientation and observations having similar pattern parameters were grouped together by K-means non-hierarchical clustering of observations according to McQueens algorithm [17]. For this study, the EDW's, were grouped into three clusters for each crack growth direction (T-1, T-2, T-3 and L-1, L-2, L-3). Statistical significance of the difference between clusters was determined by multivariate analysis of variance (Wilks test, $p < 0.05$). Differences between individual variables between clusters were determined by univariate analysis of variance (Tukey's multiple comparison, $p < 0.05$).

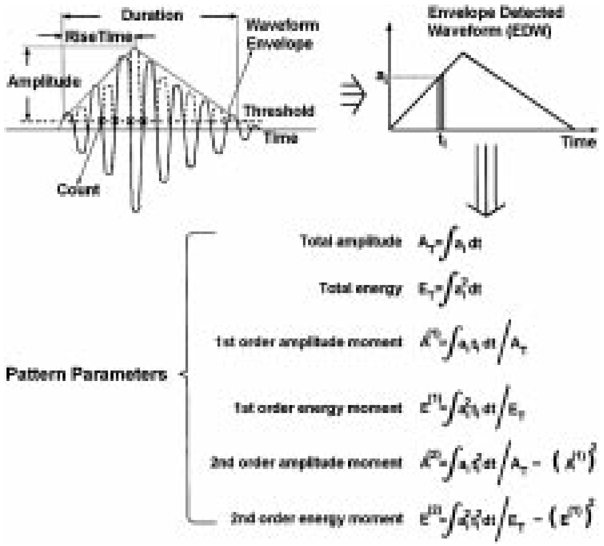

*Figure 4* Schema of an AE waveform (or hit) and the extracted waveform features, i.e. amplitude, duration, rise time and counts. Based on the extracted waveform features, the envelope detected waveform (EDW) is constructed. The six pattern parameters characterizing the shape of the EDW are obtained by integration.

## 3. Results

### 3.1. Fracture toughness and acoustic emission

The fracture toughness, $K_c$, of the transverse and longitudinal specimens were $3.47 \pm 0.40$ MNm$^{-3/2}$ and $1.71 \pm 0.37$ MNm$^{-3/2}$ (mean ± standard deviation), respectively. The fracture toughness of the transverse specimens was significantly greater than that of the longitudinal specimens ($p < 0.05$).

For both the transverse and longitudinal specimens, the first AE waveform or hit generally occurred prior to the peak load at which crack propagation started (Fig. 5). In both crack growth orientations, as the crack front advanced, the load decreased and the total number of AE hits increased (Fig. 5). The load history of the transverse specimens was marked by sharp stepwise descents in load that were closely linked with sharp stepwise increases in the total number of AE hits (Fig. 5a).

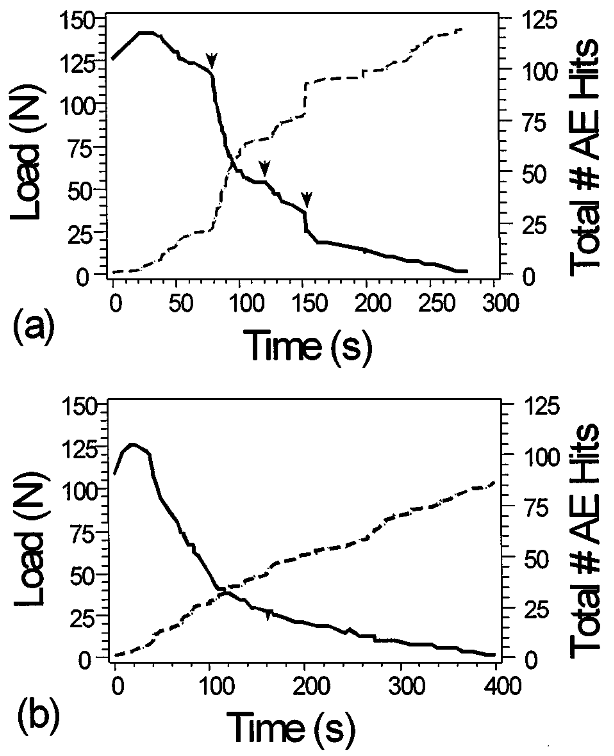

*Figure 5* Typical behavior of load versus time (unbroken line) and total number of acoustic emission hits versus time (dashed line) for (a) transverse and, (b) longitudinal specimens. Zero time is set as the time when the first acoustic emission hit (waveform) was received. The first AE waveform generally occurred prior to peak load after which crack propagation occurred. The load decreased and the total number of AE hits increased with advance of the crack front. The arrowheads mark the onset of stepwise decreases in the load history and corresponding increase in the total number of AE hits in the transverse specimen.

In contrast to the transverse specimens, the longitudinal specimens exhibited a smooth decrease in the load-time curve following attainment of peak load with a smooth increase in the total number of AE hits (Fig. 5b).

## 3.2. Histology

### *3.2.1. Transverse specimens*

Qualitative observations of the sections taken through the fracture plane revealed that the predominant mode of damage for the transverse specimens was diffuse damage in the form of excessive stain uptake that appeared bright under epi-fluorescence and dark under transmitted light. Missing fragments of osteons, interstitial tissue and bundles of osteons were also observed on this section (Fig. 6). The missing bone fragments on one fracture surface were generally found to be adherent to the mating fracture surface.

In contrast to the section taken through the fracture plane, the sections taken approximately 0.85 mm above and below the fracture plane exhibited damage in the form of linear microcracks. In some cases, linear microcracks coalesced into macrocracks running across the thickness of the specimen (Fig. 7a). The microcracks appeared to run along and across lamellae both in the interstitial tissue and in the osteons (Fig. 7b).

The numerical density of microcracks, classified by microstructural location, is given in Table I for the transverse specimens. There were significantly more

TABLE I Microcrack density (Cr.De., #/mm$^2$) based on microstructural location (mean ± standard deviation)

| | Interstitial Tissue | Cement Lines | Osteons | Total |
|---|---|---|---|---|
| Transverse Specimens | 9.4 ± 3.6* | 1.2 ± 1.0 | 2.2 ± 1.7 | 12.8 ± 5.2 |
| Longitudinal Specimens | 7.0 ± 2.4* | 1.0 ± 1.1 | 2.9 ± 0.8§ | 10.9 ± 4.1 |

*Cr.De. is highest in the interstitial tissue for both the transverse and the longitudinal specimens ($p = 0.04$, Mann-Whitney).

§Cr.De. is higher in the osteons than in cement lines only for the longitudinal specimens ($p = 0.1$, Mann-Whitney).

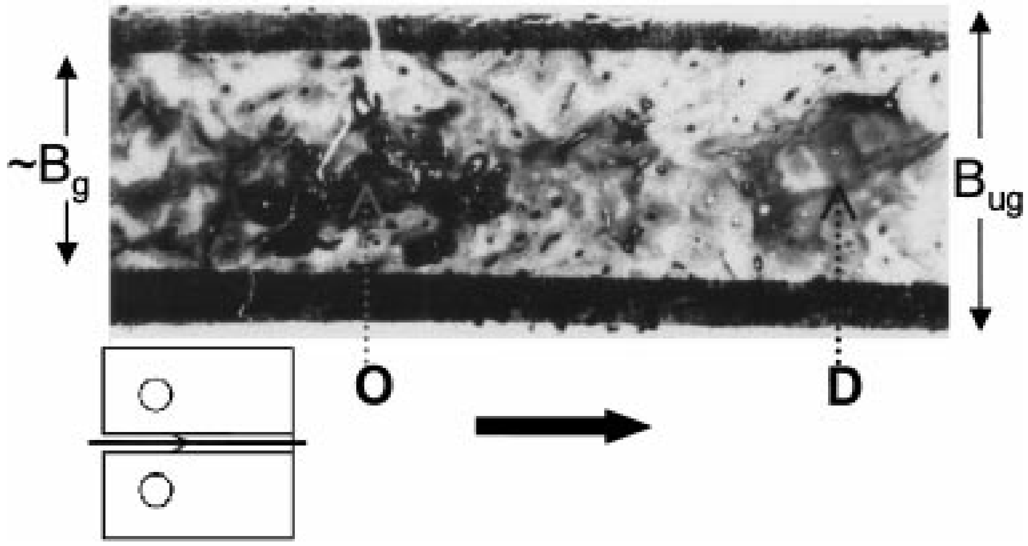

*Figure 6* Section taken through the fracture plane of a transverse human cortical bone specimen stained with 1% basic fuchsin. The schema in the lower left corner shows the location where the fracture plane section was taken. The two dark strips along the width, W, are the grooves. The direction of crack propagation is from left to right. Clouds of densely stained regions (D) were observed. In addtion, missing osteons and interstitial tissue fragments (O) were also observed. The missing material was associated with the opposite fracture surface.

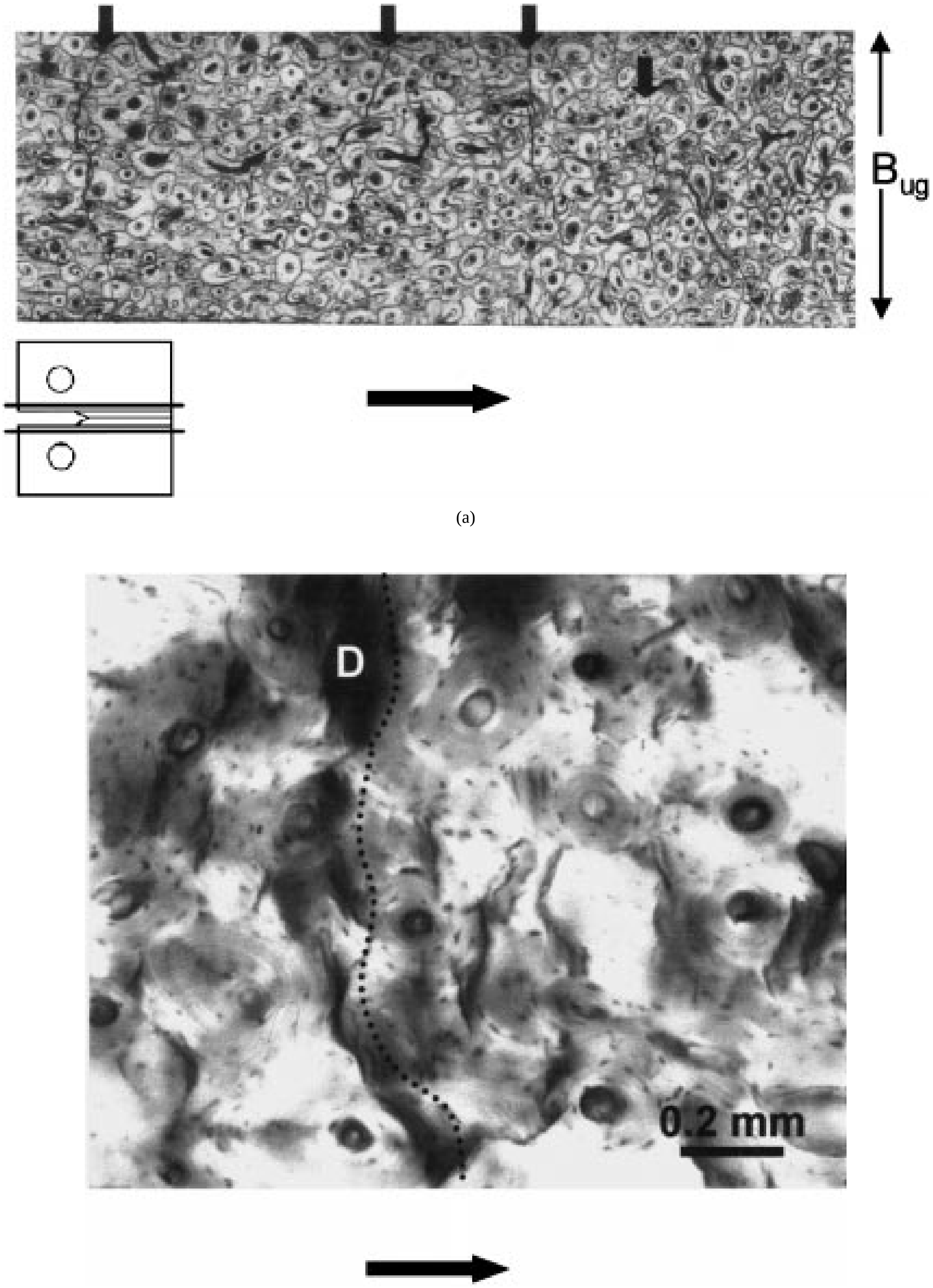

(a)

(b)

*Figure 7* (a) Histological section taken about 0.85 mm away from the fracture plane of a transverse specimen. The schema in the lower left corner shows the locations where the 0.85 mm sections were taken. The coalescence cracks running across the thickness of the specimen are shown by arrows; (b) Higher magnification image of a histological section taken about 0.85 mm away from the fracture plane of a transverse specimen. Linear microcracks were generally aligned perpendicular to the crack growth direction. The microcracks linked up to form the coalescence cracks (dotted line), as also shown in Fig. 7a. The majority of the linear microcracks were observed within the interstitial tissue. Diffuse damage (D) was also present in the section.

microcracks in the interstitial tissue than along the cement lines ($p < 0.05$) and in the osteons ($p < 0.05$). Cr.De. in the osteons was not significantly different than that in the cement lines ($p = 0.33$).

### *3.2.2. Longitudinal specimens*

The histology of the longitudinal specimens revealed that the fracture plane was banded by diffuse damage (Fig. 8a). In addition to diffuse damage, extensive

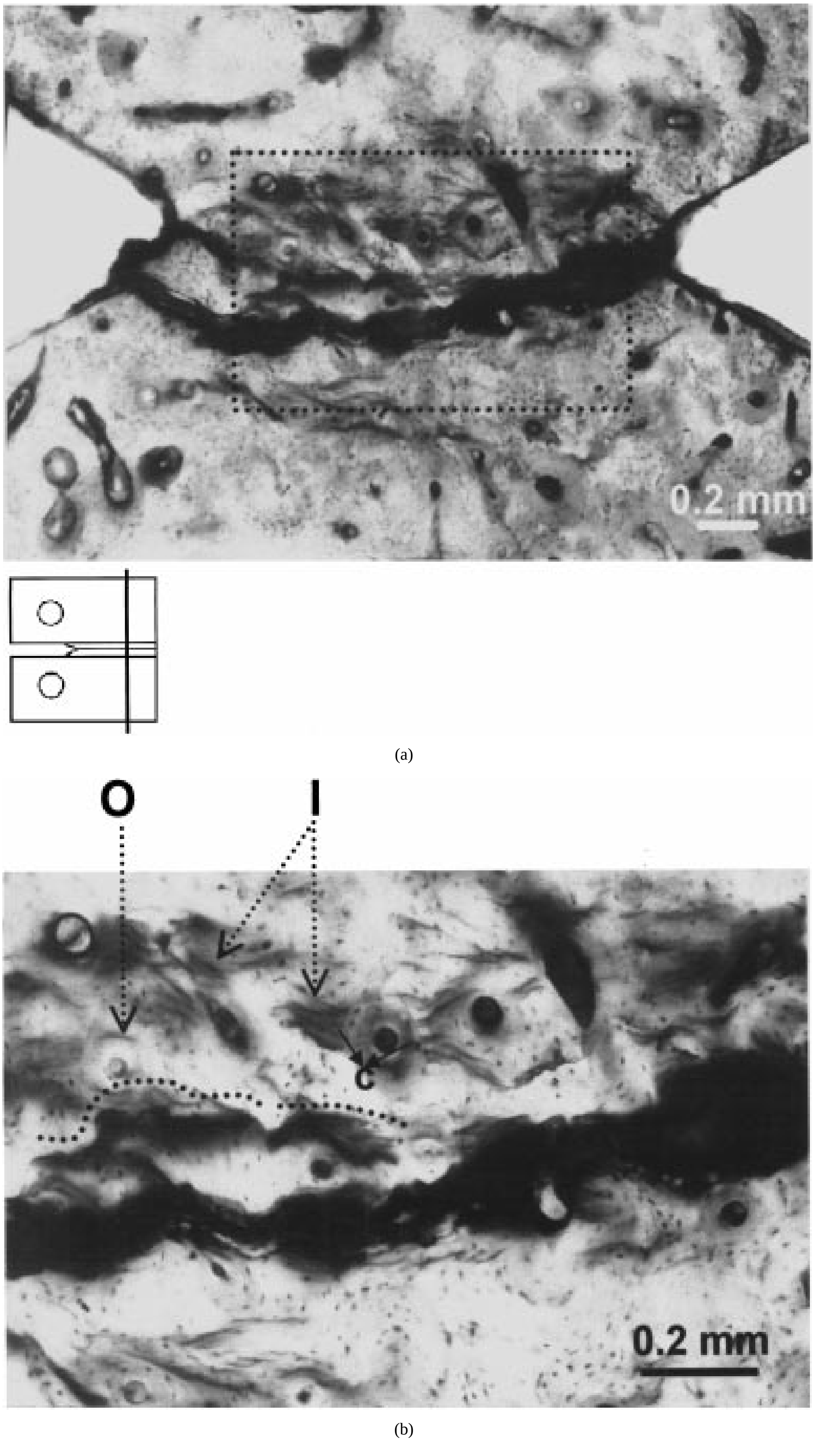

(a)

(b)

*Figure 8* (a) A section taken perpendicular to crack propagation direction of a longitudinal specimen. The direction of crack propagation is into the plane of the page. The fracture plane is banded by diffuse damage as observed by diffuse staining; (b) Higher magnification image of the framed region in Fig. 8a. Damage parallel to the fracture plane can be observed as separations along osteonal and interstitial lamellae (O and I, respectively). Microcracks generally arrested at cement lines (c). Coalescence of cracks (dotted line) parallel to fracture plane were also observed for the longitudinal specimens.

microcracking, that is, separations along the osteonal lamellae and within the interstitial lamellae, was observed (Fig. 8b). The microcracks in the longitudinal specimens were observed to occur primarily along lamellar interfaces, in contrast to the microcracks in the transverse specimens that occurred both along and across lamellae. The microcracks in the interstitial tissue generally were observed to arrest at cement lines and did not cross osteonal boundaries. Similarly, the microcracks within osteons were generally observed to be confined within the osteons and did not cross into the interstitial tissue.

Coalescence of linear microcracks was also observed for the longitudinal specimens (Fig. 8b). These coalescence cracks were generally parallel to the fracture plane and occurred in the form of linking up of the cracks within the interstitial matrix through osteonal lamellae or cement lines.

The numerical density of microcracks, classified by microstructural location, is given in Table I for the longitudinal specimens. There were significantly more microcracks in the interstitial tissue than along the cement lines ($p < 0.05$) and in the osteons ($p < 0.05$). In contrast to the transverse specimens, the Cr.De. in the osteons was greater than that in the cement lines for the longitudinal specimens ($p < 0.01$).

### 3.3. Identification of failure modes by clustering of acoustic emission waveforms

For the transverse specimens, the three clusters of AE waveforms (T-1, T-2, T-3) were significantly different when all six variables were considered together ($p = 0.001$). For example, Fig. 9a shows the amplitude versus the 1st moment of amplitude plot for the three clusters. The clusters can be observed to be distinct. There were significant differences between each of the six corresponding variables of any two clusters for the transverse specimens ($p < 0.05$) (Table II).

With an increase in total energy, $E_T$, the total number of EDW's in the cluster decreased. For example, the highest energy cluster (T-3) occurred only 15 times during fracture of the 4 transverse specimens. The T-3 cluster waveforms were generally concomitant with the onset of stepwise load descents (Fig. 5a). In contrast to the T-3 cluster, the total number of EDW's in the T-1 cluster was 455 and in the T-2 cluster was 129 during fracture of the 4 transverse specimens (Table II).

For the longitudinal specimens, the three clusters of AE waveforms (L-1, L-2, L-3) were also significantly different ($p = 0.001$) when all six variables were considered together (Fig. 9b). Similar to the transverse specimens, a significant difference ($p < 0.05$) between each of the six corresponding variables of any two clusters for the longitudinal specimens was found (Table II).

The six variables, CO, $E_T$, $A^{(1)}$, $E^{(1)}$, $A^{(2)}$, $E^{(2)}$, of the EDW's were also compared between the transverse and longitudinal clusters. All of the six variables were significantly greater in T-1, T-2 and T-3 than in L-1, L-2 and L-3, respectively ($p < 0.05$).

TABLE II Pattern parameters of the three clusters obtained by K-means non-hierarchical clustering method for the transverse and longitudinal specimens (mean ± standard deviation)

| Transverse Specimens | T-1 | T-2 | T-3 |
|---|---|---|---|
| Total # of EDW's in the cluster | 455 | 129 | 15 |
| CO | $8.2 \pm 6.3$ | $31.8 \pm 9.0$ | $70.8 \pm 21.6$ |
| $E_T(\times 10^3)$ (dB$^2\mu$s) | $52.2 \pm 54.6$ | $452.7 \pm 236.4$ | $1830.1 \pm 438.5$ |
| $A^{(1)}$ ($\mu$s) | $13.0 \pm 9.7$ | $64.7 \pm 26.1$ | $195.2 \pm 37.5$ |
| $E^{(1)}$ ($\mu$s) | $11.0 \pm 7.8$ | $52.6 \pm 23.3$ | $151.5 \pm 27.9$ |
| $A^{(2)}$ ($\mu$s$^2$) | $95 \pm 140$ | $1886 \pm 1580$ | $17994 \pm 8741$ |
| $E^{(2)}$ ($\mu$s$^2$) | $153 \pm 225$ | $3015 \pm 2533$ | $28618 \pm 13673$ |
| Longitudinal Specimens | L-1 | L-2 | L-3 |
| Total # of EDW's in the cluster | 225 | 48 | 15 |
| CO | $3.6 \pm 2.3$ | $13.4 \pm 4.3$ | $25.5 \pm 5.1$ |
| $E_T(\times 10^3)$ (dB$^2\mu$s) | $13.4 \pm 10.4$ | $72.7 \pm 22.4$ | $211.0 \pm 48.5$ |
| $A^{(1)}$ ($\mu$s) | $5.0 \pm 3.0$ | $18.0 \pm 5.8$ | $34.2 \pm 6.1$ |
| $E^{(1)}$ ($\mu$s) | $4.3 \pm 2.6$ | $15.1 \pm 6.2$ | $26.8 \pm 4.7$ |
| $A^{(2)}$ ($\mu$s$^2$) | $11 \pm 13$ | $122 \pm 63$ | $530 \pm 221$ |
| $E^{(2)}$ ($\mu$s$^2$) | $17 \pm 21$ | $194 \pm 98$ | $847 \pm 349$ |

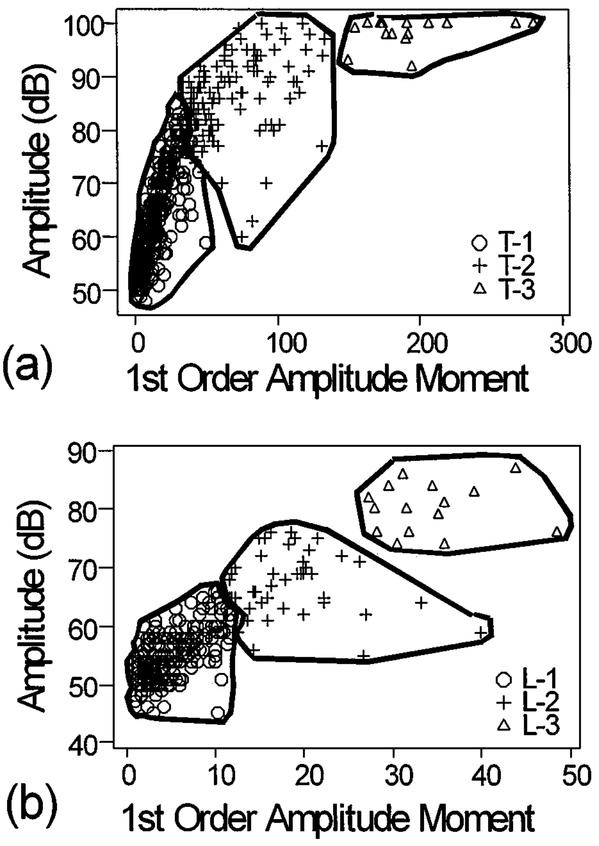

*Figure 9* The clusters obtained by K-means clustering of the envelope detected waveforms for (a) transverse, and (b) longitudinal specimens.

The manner in which the AE waveform clusters accumulated was different between the transverse and longitudinal crack growth direction specimens. For the transverse specimens, the T-1 and T-2 clusters generally accumulated continuously, but with periodic sharp (and synchronous) increases (Fig. 10a). The T-3 cluster generally occurred at these sharp increases and was quiescent at other times. In contrast to the transverse specimens, the three AE waveform clusters for the longitudinal specimens accumulated continuously and with no apparent relationship to one another (Fig. 10b).

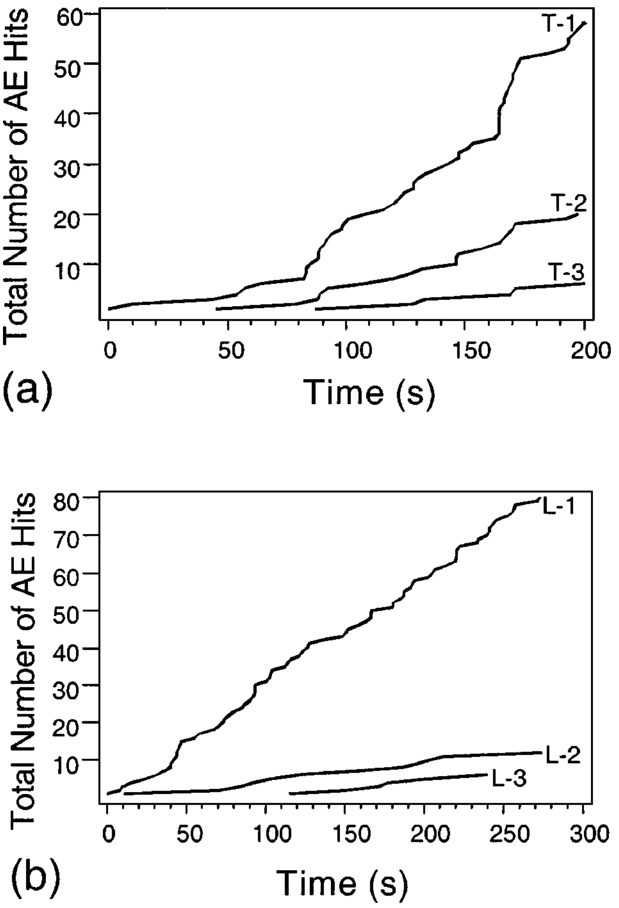

*Figure 10* Temporal sequence of the clusters of AE hits for: (a) a transverse specimen; and (b) a longitudinal specimen.

## 4. Discussion

The interaction of microcracks with the microstructure and their coalescence was investigated by conducting fracture toughness tests on cortical bone tissue with crack growth transverse and longitudinal to osteon orientation. Differences in fracture toughness, AE patterns and histological appearance of the damage were observed for the two crack growth directions. Thus, this study suggests that the manner in which microcracks initiate and accumulate in the two crack growth directions is not the same, which provides insight into the observed difference in the fracture resistance of cortical bone tissue in the two crack growth directions.

### 4.1. Fracture toughness

In this study, it was found that the fracture toughness of human cortical bone was significantly greater in the transverse direction compared with the longitudinal direction. In spite of its clinical relevance [18, 19], little is known about the fracture toughness of human cortical bone for crack growth transverse to osteons [20, 21]. The transverse fracture toughness obtained in this study is less than that reported by Zioupos and Currey [21]. However, the longitudinal fracture toughness, $K_c$, obtained in this study is in general agreement with those reported previously [22–25]. Discrepancies between the reported fracture toughness values may be attributed to differences in the method by which the fracture toughness is calculated, differences in specimen geometry, loading rate, bone age, and bone source (tibia versus femur). Overall, the ratio of the transverse fracture toughness to the longitudinal toughness in this study was approximately two, which is consistent with that reported for bovine bone [13].

### 4.2. Histology

In the current study, histological examination of both the transverse and the longitudinal specimens demonstrated that the primary form of damage at the fracture plane was diffuse damage (Figs 6 and 8). Diffuse damage patterns have been associated with artificially induced stress concentrations by others [26, 27]. In contrast, linear microcracks were observed in locations away from the fracture plane for both the transverse and the longitudinal specimens (Figs 7b and 8b). Different failure modes at and near the fracture plane may be explained by consideration of the process zone at the tip of the macrocrack. The stress level within the process zone is generally well above the yield stress. Such a stress state can be expected to result in generalized, ultrastructural level damage (i.e., diffuse damage) at the fracture plane. However substantially lower stresses exist outside the process zone, and, thus, comparably less diffuse damage is expected to occur in the neighboring sections.

The total microcrack densities of the transverse and longitudinal specimens were 12.8 ± 5.2 #/mm$^2$ and 10.9 ± 4.1 #/mm$^2$, six to 40 times higher than that reported for *in vivo* microcrack densities [7, 8, 27]. The difference in these microcrack densities strongly suggests that the majority of the microcracks observed in this study were due to damage accumulation during the fracture process.

Previous investigations have reported that the majority of the *in vivo* microcracks were observed within the interstitial tissue [7, 8]. Consistent with these previous studies, it was found in this study that the majority of fracture induced microcracks outside the process zone occurred within the interstitial tissue for both the transverse and the longitudinal crack growth directions (Table I).

### 4.3. Sources of identified acoustic emission waveform clusters

The shape of the acoustic emission waveforms is a function of the elastic properties of the medium in which the wave travels, the location of the transducers, the shape and size of the specimen, and the frequency response of the data acquisition system. Therefore, it must be noted that the reported results of the acoustic emission analyses are specific to the test conditions defined in this study.

In the current study, significantly different AE waveform clusters were recorded, implying the existence of different failure modes. The waveforms of T-3 and L-3 clusters were very low in number and very high in energy content when compared with the T-2, T-1, L-2 and L-1 clusters (Table II). These observations suggest that waveforms belonging to the T3 and L3 clusters were associated with growth of the main crack. Furthermore, the concomitance of the T-3 cluster waveforms with the onset of stepwise load descents (Fig. 5a) strongly suggests an association of the T-3 cluster with incremental growth of the main crack.

The high number of AE waveforms in the T-1, T-2, L-1 and L-2 clusters (Table II) suggests that these clusters emanated from the formation of linear microcracks and diffuse damage. Histologically, linear microcracks were observed on the fracture plane as well as on the sections above and below the fracture plane. In contrast, diffuse damage was observed primarily on the fracture plane sections. Thus, it may be reasonable to expect that there would be a higher number of AE waveforms emanating from the occurrence of linear microcracks than from the occurrence of diffuse damage. It is therefore speculated that the T-1 and L-1 clusters are originating from the formation of linear microcracks while the T-2 and L-2 clusters are associated with diffuse damage since there were higher number of waveforms in T-1 and L-1 clusters than in T-2 and L-2 clusters, respectively.

The AE waveforms were grouped into three clusters based on the observed failure modes (diffuse damage, microcracks, and growth of the main crack). In future studies, it may be appropriate to group the AE waveforms into more than three clusters if a more detailed description of failure modes becomes available. In this study, the assignment of the AE clusters to histologically identifiable damage modes is speculative and needs to be rigorously validated. To accomplish such a validation, the assignment of an AE waveform to a damage mode requires demonstration of that damage mode selectively. Such validations have been conducted on synthetic composite materials [28]. For cortical bone tissue, demonstration of a particular damage mode without interference from other damage would be difficult.

The temporal records of AE data revealed that the waveforms of the T-1 and T-2 clusters occurred and accumulated synchronously for the transverse specimens in that the sharp periodic increases were synchronous (Fig. 10a). This observation, along with the observation that T-3 occurs only during stepwise load descents, suggests that the tissue at the tip of the main crack gradually weakens due to continuous accumulation of diffuse damage and linear microcracks and is then followed by the growth of the main crack.

In contrast, for the longitudinal specimens, the waveforms of the three clusters occurred and accumulated independently of one another (Fig. 10b). These results suggest that, for the longitudinal specimens, there was no temporal relationship between the accumulation of diffuse damage and linear microcracks and growth of the main crack.

Comparing the total energies of the waveform clusters between the transverse and longitudinal specimens, it can be seen that the total energy of the T-1, T-2, and T-3 clusters were significantly higher than that of the L-1, L-2, and L-3 clusters, respectively (Table II). This observation is consistent with that found for synthetic composite materials [28] in that the energy required to separate lamellae would be expected to be considerably less than the energy required for transverse failure of lamellae. Together, the higher energy content of the transverse waveform clusters reflects the greater crack growth resistance transversely as reflected by the higher fracture toughness for the transverse specimens.

In conclusion, this study has demonstrated that acoustic emission analysis in combination with histological examination of damage can be a useful method to evaluate the development of damage during fracture of bone from a stress concentration.

## Acknowledgements

This study was supported by The Musculoskeletal Transplant Foundation and NIH Grant AR 43785. The Musculoskeletal Transplant Foundation provided human tissues. We also thank Ms. Teresa Pizzuto for her contributions in the histological staining.

## References

1. B. HARRIS, F. J. GUILD and C. R. BROWN, *J. Mater. Sci.* **10** (1975) 2050.
2. K. L. REIFSNIDER, in "Fatigue of Composite Materials," edited by K. L. Reifsnider (Elsevier, New York, 1991) p. 11.
3. H. L. FROST, *Henry Ford Hosp. Med. Bull.* **8** (1960) 25.
4. K. J. JEPSEN and D. T. DAVY, *J. Biomech.* **30** (1997) 891.
5. K. J. JEPSEN, D. J. KRZYPOW, T. DUTTA ROY and T. PIZZUTO, in "Transactions of the Orthopaedic Research Society" (Anaheim, 1999) p. 236.
6. M. B. SCHAFFLER, E. L. RADIN and D. B. BURR, *Bone* **11** (1990) 321.
7. M. B. SCHAFFLER, K. CHOI and C. MILGROM, *ibid.* **17** (1995) 521.
8. T. L. NORMAN and Z. WANG, *ibid.* **20** (1997) 375.
9. G. C. REILLY and J. D. CURREY, in Proceedings of the 11th Conference of the European Society of Biomechanics, Toulouse, 1998, p. 1.
10. P. ZIOUPOS, X. T. WANG and J. D. CURREY, *Clin. Biomech.* **11** (1996) 365.
11. A. C. COURTNEY, W. C. HAYES and L. J. GIBSON, *J. Biomech.* **29** (1996) 1463.
12. ASTM E399-90 Standard Test Method for Plane-Strain Fracture Toughness of Metallic Materials, in Annual Book of ASTM Standards Vol 03.01. (American Society for Testing and Materials, Philadelphia, 1990) p. 407.
13. J. C. BEHIRI and W. BONFIELD, *J. Biomech.* **22** (1989) 863.
14. T. L. NORMAN, D. VASHISHTH and D. B. BURR, *ibid.* **25** (1992) 1489.
15. D. B. BURR and T. STAFFORD, *Clin. Orthop.* **260** (1990) 305.
16. K. YAMAGUCHI, H. OYAIZU, J. JOHKAJI and Y. KOBAYASHI, in "Acoustic Emission: Current Practice and Future Directions," ASTM STP 1077, edited by W. Sachse, J. Roget and K. Yamaguchi (American Society for Testing and Materials, Philadelphia, 1991) p. 123.
17. R. A. JOHNSON and D. W. WICHERN, in "Applied Multivariate Statistical Analysis" (Prentice-Hall, Englewood Cliffs, 1988).
18. A. G. APLEY and L. SOLOMON, in "Concise System of Orthopaedics and Fractures" (Butterworth and Heinemann, Cambridge, 1994).
19. D. L. PETERSON, J. S. SKRABA, J. M. MORAN and A. S. GREENWALD, *J. Orthop. Res.* **1** (1984) 244.
20. J. W. MELVIN, *J. Biomech. Eng.* **115** (1993) 549.
21. P. ZIOUPOS and J. D. CURREY, *Bone* **22** (1998) 57.
22. T. L. NORMAN, D. VASHISHTH and D. B. BURR, *J. Biomech.* **28** (1995) 309.
23. W. BONFIELD, J. C. BEHIRI and B. CHARALAMBIDES, in "Biomechanics: Current Interdisciplinary Research," edited by S. M. Perren and E. Schneider (Martinus-Nijhoff, Dordrecht, 1985) p. 185.

24. D. VASHISHTH, J. C. BEHIRI and W. BONFIELD, *J. Biomech.* **30** (1997) 763.
25. D. D. RAFTOPOULOS, J. MEISSNER, M. KONSTAGDOUTOS and E. E. GDOUTOS, *Int. J. Fract.* **91** (1998) L51.
26. P. ZIOUPOS and J. D. CURREY, *J. Mater. Sci.* **29** (1994) 978.
27. M. B. SCHAFFLER, W. C. PITCHFORD, K. CHOI and J. M. RIDDLE, *Bone* **15** (1994) 483.
28. R. KRAUS, A. PAYER and W. WILKE, *J. Mater. Sci.* **28** (1993) 4047.

*Received 24 January*
*and accepted 2 May 2000*